Proceedings of ASME Turbo Expo 2011
GT2011
June 6-10, 2011, Vancouver, British Columbia, Canada

GT2011-45210

NEAR AND FAR-FIELD INVESTIGATIONS OF SUPERSONIC JET NOISE PREDICTIONS USING A COUPLED LES AND FW-H EQUATION METHOD

James P. Erwin
Combustion Research and Flow Technology, Inc
Pipersville, PA 18947, United States
Email: jerwin@craft-tech.com

Neeraj Sinha
Combustion Research and Flow Technology, Inc
Pipersville, PA 18947, United States
Email: sinha@craft-tech.com

ABSTRACT

The hot supersonic exhausts of gas turbine engines on military aircraft generate dangerously high noise levels. The noise levels associated with operating these engines are harmful to aircraft carrier deck personnel as well as detrimental to ship and aircraft structures. In this paper, the supersonic jet exhaust is simulated using Large Eddy Simulation (LES), and the Ffowcs Williams and Hawkings (FW-H) equation transforms the LES solution to an acoustic solution in the far-field. A Mach 1.5 laboratory jet test at United Technologies Research Center - Acoustics Research Tunnel is used as validation for the LES/FW-H method. A grid refinement study was performed with the objective of determining the requirements for accurate noise predictions. The finest grid resolution yields the best near and far-field acoustic prediction. A second LES/FW-H validation case is shown for a twin jet experiment that was performed in the anechoic chamber at University of Mississippi's National Center for Physical Acoustics (NCPA). The LES/FW-H method is applied to the higher complexity heated twin jet with faceted nozzle profiles, demonstrating the applicability of the method over a wider range of flow regimes. The far-field noise prediction agrees very well with the NCPA experiment, including the prediction of broadband shock associated noise and jet screech.

NOMENCLATURE

c_0 Sound speed in undisturbed medium
dA Differential area element on FW-H surface
D_J Jet nozzle exit diameter
FW-H Ffowcs Williams and Hawkings
FF1A Formulation 1A of Farassat
LES Large Eddy Simulation
$\vec{L}$ Redefined loading vector
p Pressure on FW-H surface
p_0 Pressure in undisturbed medium
p' Perturbation pressure, $p' = p - p_0$
$p'_D(\vec{x},t)$ Dipole-like far-field acoustic pressure
$p'_M(\vec{x},t)$ Monopole-like far-field acoustic pressure
r Distance between dA and observer, $r = |\vec{y} - \vec{x}|$
RANS Reynolds Averaged Navier Stokes
ρ Density on FW-H surface
ρ_0 Density of undisturbed medium
SPL Sound pressure level (dB, ref. 20 μPa)
St_D Strouhal number based on Jet nozzle diameter
t Observer time
τ Retarded time
$\vec{U}$ Redefined velocity vector
$\vec{u}$ Velocity vector of fluid on FW-H surface
$\vec{x}$ Observer coordinate vector
$\vec{y}$ dA coordinate vector

INTRODUCTION

Noise reduction of military aircraft is one of the primary goals of the United States Navy. The hot supersonic exhausts of military gas turbine engines generate noise levels that are dangerous to the aircraft launch personnel, as well as harmful to the structural integrity of the aircraft and ship deck structures. Modern tactical aircraft operate at full power settings very close to sailors, exposing the sailors to unhealthy noise levels. A recent Naval Research Advisory Committee Report (2009) on jet noise reduction noted that, "Flight deck noise is a serious health risk" which must be addressed. The noise levels on Navy flight decks often exceed the capability of current hearing protection for personnel [1]. A numerical method to predict the supersonic jet noise can aid in the design of practical and effective noise reduction concepts.

Noise reduction concepts attached to the nozzle can modify the jet noise sources, but they can also be expensive to build and test at laboratory and full scale. Mixing chevrons, water

injection, microjet control, and plasma actuators have demonstrated potential in reducing jet noise [2–5]. Large Eddy Simulation (LES) is a numerical method that can be used to predict the noise source mechanisms in a supersonic jet plume. LES can predict the effect of noise reduction concepts on jet noise sources such as Eddy Mach Wave radiation, broadband shock associated noise, and jet screech. However, propagating the sound waves to the far-field with LES is still too expensive due to grid resolution limitations. Presented in this paper is an alternate hybrid method, where only the noise generating region of the flow is simulated with LES, and the noise in the far-field is predicted with a transformation using the Ffowcs Williams and Hawkings (FW-H) equation.

In hybrid LES/FW-H simulations, the LES is coupled to the far-field acoustic signature using the FW-H equation [6–9]. The near-field flow variables (ρ, $\vec{u}$, and p) are recorded in the linear wave propagation region on a fictitious FW-H surface. This surface is then used by the far-field acoustic solver to calculate overall sound pressure levels and sound pressure level spectra at far-field observer (virtual microphone) locations. The frequency resolution and overall accuracy of the far-field noise is directly related to the frequency resolution and accuracy of the LES in the noise source regions.

The aim of the present paper is to describe the complete LES/FW-H method and show its applicability to supersonic jet noise. In the next sections, the LES code and FW-H method is outlined, followed by the coupling techniques for FW-H surfaces with supersonic jet plumes. Two supersonic laboratory jet cases are then presented that demonstrate the method, including an isothermal Mach 1.5 jet and also a heated twin jet configuration.

CRAFT CFD® LES CODE

CRAFT Tech's LES and DNS capability is implemented within the well-established CRAFT CFD® structured grid, Navier Stokes solver, which has been used extensively for the evaluation of jet noise attenuation concepts for military gas turbine engines [10]. A hybrid RANS/LES (HRLES) method which was originally developed for cavity flows [11] can be implemented for supersonic jet exhausts. A low-dissipation fifth-order upwind biased reconstruction procedure is used with Roe's shock capturing, approximate Reimann solver [12, 13]. For LES, subgrid stresses are modeled by solving a transport equation for the subgrid kinetic energy as developed by Kim and Menon [14]. The HRLES model analyzes the turbulent energy spectrum of every point in the flowfield and the eddy viscosity is computed based on the unresolved portion of this spectrum. The code is parallelized using domain decomposition and achieves nearly linear speed-up on several large supercomputers. A DNS study of subsonic and supersonic turbulent free shear flow [13] demonstrates the capability of the fifth-order reconstruction scheme. For a fixed grid resolution, the algorithm demonstrates minimal numerical dissipation and dispersion relative to other schemes.

Supersonic jet plumes present many challenges for LES. There are a large range of flow scales that vary from the lip of the nozzle, where the eddy scales are very fine and the time scales are short, to many jet diameters downstream where the turbulence is fully developed, the eddy scales are larger and time scales are longer. The capability of CRAFT CFD® to resolve this range of scales at modest grid resolutions [15] has been shown to produce accurate far-field noise predictions when coupled with the far-field acoustic solver. An O-H type grid topology is used for jet plume simulations and is illustrated in Figure 1. The H grid extends along the axis of the jet and eliminates the centerline pole. The O grids allow for finely resolved nozzle lip resolution and efficient acoustic wave propagation away from the shear layer. Care is taken when constructing the O-H grids, ensuring smooth transition from the H to the O grid and modest grid stretching to prevent numerical dissipation.

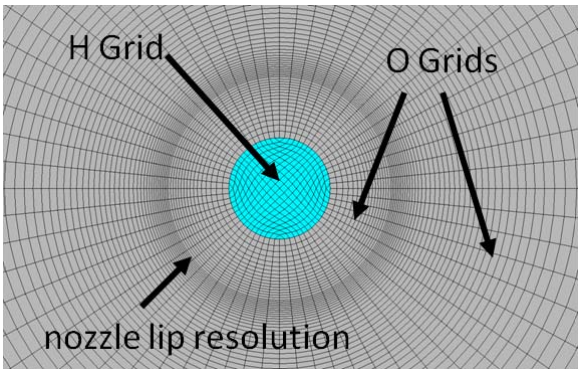

FIGURE 1. O-H GRID TOPOLOGY

FAR-FIELD ACOUSTIC SOLVER

The acoustic signature at far-field microphone locations can be calculated through a transformation of the LES solution. The transformation solves the FW-H equation using Farassat's Formulation 1A (FF1A) [16, 17]. The FW-H equation is an exact rearrangement of the continuity and Navier Stokes equations into an inhomogeneous wave equation. An in-depth analysis of the FW-H and Kirchhoff methods is given by Brentner and Farassat [18]. For a stationary observer and acoustic data surface, FF1A can be written as

$$4\pi p'_M(\vec{x},t) = \int_{f=0}\left[\frac{\rho_0 \dot{U}_n}{r}\right]_{ret} dA \tag{1}$$

$$4\pi p'_D(\vec{x},t) = \frac{1}{c_0}\int_{f=0}\left[\frac{\dot{L}_r}{r}\right]_{ret} dA + \int_{f=0}\left[\frac{L_r}{r^2}\right]_{ret} dA \tag{2}$$

where the monopole-like term given by Eqn. 1 and the dipole-like term is given by Eqn. 2. The total noise at any observer location is given by $p'(\vec{x},t) = p'_M(\vec{x},t) + p'_D(\vec{x},t)$. A dot over a variable implies retarded time differentiation of that variable. In

the current method, a second order backwards difference is used. FF1A neglects the computationally expensive volume source term, and the monopole and dipole-like terms are surface integration terms that are assumed to enclose all of the non-linear noise generating mechanisms of the flow. A simplification is adopted by di Francescantonio [19], where the redefined loading and velocity vectors are given as $L_i = p'\hat{n}_i + \rho u_i u_n$ and $U_i = \rho u_i/\rho_0$.

The FW-H surface is defined by $f = 0$, where $\hat{n}$ is the unit outward normal to the surface for each differential area segment dA. Equations 1 and 2 are evaluated at the retarded time. The contribution of the retarded time flowfield to the noise at some later observer time is determined via the source time algorithm, which simplifies to $t = \tau + r/c_0$ for a stationary FW-H surface and observer. At every retarded timestep, each differential area contributes noise to the observer at unique times. The observer noise at any specified time is the summation of each differential area's noise contribution after it is interpolated to the specified observer time.

The original formulation requires the density of the fluid which can be obtained directly from the LES [17]. A second formulation based on pressure is used in the current work [20], where the density is now purely a function of the perturbation pressure, $\rho = \rho_0 + p'/c_0^2$, where ρ_0 is the density of the undisturbed medium. This formulation has been shown to improve noise calculations in the case where entropy fluctuations cross the FW-H surface [21].

FW-H Acoustic Data Surfaces

During the jet simulations, time histories of the acoustic variables are recorded in the near-field with a permeable FW-H surface. The current implementation of the FW-H equation requires the surface to exist in only the linear wave propagation region of the flowfield. Figure 2 is an example of how a FW-H surface is placed around the jet plume, exhausting from left to right. Shown in the figure are contours of vorticity (color), and contours of dilatation (greyscale) that visualize the acoustic field. The surface (shaded grey) is shaped like a cone and encloses most of the noise generating regions of the jet plume, except the sources that exit the outflow of the domain. The end of the acoustic data surface is left open to allow for vorticity to exit the domain into the buffer zone. The extent of the LES downstream is currently limited by maximum allowable grid size, and therefore the surface must be left open to allow for the vorticity to exit the domain without adding spurious noise to the FW-H transformation.

There are many open-ended questions regarding the proper use and placement of FW-H surfaces with free jets. In the current work, there is no end cap surface located at the downstream end of the jet plume. An in-depth investigation of the presence of an end cap, including end cap averaging procedures, has been performed by Mendez *et. al.* [21]. An end cap averaging procedure, developed by Shur *et al.* [22], has been used by various groups with success in eliminating spurious low frequency noise when compared with using a single or no end cap. There is no conclusive evidence that suggests the use of an end cap improves far-field noise predictions for all scenarios. The improvements

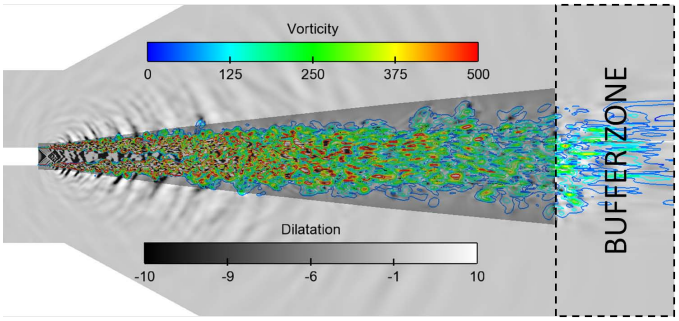

FIGURE 2. SCHEMATIC OF JET DOMAIN SHOWING CONTOURS OF VORTICITY, DILATATION, AND THE LOCATION OF THE ACOUSTIC DATA SURFACE

to far-field noise predictions when using end caps, with or without the averaging technique, depend on the specific implementation [21]. If the surface extends sufficiently far downstream, negligible noise differences have been found at CRAFT Tech between averaging the end caps or using no end cap at all.

The radial location of the FW-H surface has a direct affect on the maximum frequency resolution in the far-field. In general, it should be placed as closely as possible to the shear layer without intersecting significant non-linearities. This minimizes dissipation at higher frequencies due to the relaxing grid resolution as the O grids extend outward. In Fig. 2, some vorticity is shown intersecting the acoustic data surface, but this infrequent occurrence does not seem to contaminate the far-field solution enough to warrant moving the data surface outward and sacrificing high frequency resolution. An in-depth study of the affect of FW-H surface placement on frequency resolution is given by Uzun [23]. In the current work, the surface is defined by constant O grid levels, and no spatial interpolation is performed from the LES to the surface. The maximum frequency resolution corresponds to a Strouhal number of between 1 and 2 ($St_D = fD_J/U_J$).

APPLICATION OF NUMERICAL METHOD TO JET NOISE PROBLEMS

This section briefly describes the strategy used when performing the LES/FW-H noise predictions. Although the specific operating conditions vary among unique jets, an overall "best practice" has been adopted that leads to consistent noise predictions.

The grid spacing at the nozzle lip is 0.25% of the jet exit diameter (D_J) in both the radial and axial direction. The grid is stretched away from the nozzle lip using a hyperbolic tangent function in the radial direction, and using geometric progression in the axial direction. The grid extends at least $30D_J$ downstream before rapid grid stretching in the buffer zone. The number of grid cells used in the axial direction is selected such that the axial grid spacing at the downstream end corresponds to a resolution of around $St_D = 1$. The high resolution at the lip of the nozzle is moved out radially in the downstream direction, to capture the anticipated growth of the shear layer. The azimuthal resolution of the O grid is selected such that the overall desired grid cell count

is not exceeded. The coarsest azimuthal resolution in this study is approximately 6°, and this grid will be shown to severely under-predict higher frequencies. It is clear that careful consideration must be given to the azimuthal resolution when using O-H grid topologies.

The internal nozzle calculations are performed in the RANS framework of CRAFT CFD®, and the nozzle solution at the exit plane is then interfaced into the LES domain for the unsteady calculation. For circular laboratory nozzles, axi-symmetric solutions are revolved around the jet axis and the LES begins with a laminar nozzle boundary layer solution. In general, the shear layer in the LES calculation becomes turbulent very close to the nozzle lip, so no inflow forcing is used to excite the shear layer. This has proven in the past to provide reasonable near-field and far-field results at laboratory scale [9]. To achieve statistical convergence, the laboratory simulations run at a physical time step of 5.0×10^{-7} seconds for approximately 100,000 time steps (about 10 jet flow-through cycles of a Mach 1.5 jet).

After the jet is statistically converged, the time-accurate sampling begins using second order implicit time marching and three sub-iterations per time step. Solution files are saved every 500-1000 iterations for time averaged flow-field analysis. In addition, the flow variables are written to the FW-H surface at a sampling frequency of 100 kHz. The simulation is continued until the desired low frequency resolution is achieved. Visualizing spectrograms at various locations on the FW-H surface can show how the spectral density varies with time. This ensures that the far-field noise calculation is not contaminated with low frequency signals due to start up transients, reflections from boundary conditions, and other non-physical scenarios that can lead to incorrect noise predictions.

MACH 1.5 LABORATORY JET

A Mach 1.5 laboratory jet experiment conducted at United Technologies Research Center (UTRC) Acoustics Research Tunnel (ART) is used for validation of the current methodology. Khalighi *et. al.* [24] and Schlinker *et. al.* [25] describe the jet operating conditions and laboratory setup. Nozzle exit profiles, mean and RMS flow profiles in the jet plume, and near and far-field microphone measurements are available in the literature for an ideally expanded and isothermal test case named B118.

A method-of-characteristics converging-diverging nozzle (D_J =3.0") was operated with a Mach 0.1 coflow from an open jet surrounding the primary jet noise rig. The open jet diameter is many diameters larger than the primary jet. A CRAFT CFD® RANS calculation was carried out for the internal nozzle, and solutions of Mach number and nozzle exit velocity are seen in Fig. 3 and 4. The nozzle exit profile of the RANS calculation agrees with the experimental measurements.

Mach 1.5 Laboratory Jet LES

Three levels of grid resolution were used in the current analysis. A coarse grid consisting of approximately 2.5 million cells was initially performed, but the near-field statistics did not compare well with the experimental measurements so successive grid

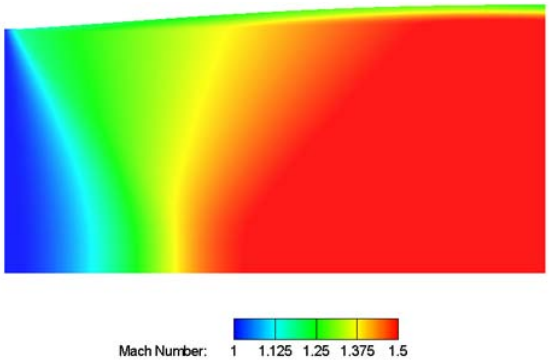

FIGURE 3. NOZZLE MACH NUMBER CONTOURS (RANS)

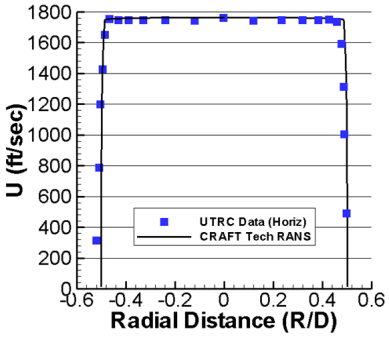

FIGURE 4. NOZZLE EXIT VELOCITY PROFILE COMPARED WITH UTRC EXPERIMENT

refinement took place. There was also a medium and fine grid calculation consisting of 8 and 20 million cells, respectively. Figure 5 and 6 are time averaged and instantaneous density and temperature solutions for the medium grid. Mach wave radiation can be seen emitting from the shear layer in the instantaneous density contours. Also, rapid growth of large scale turbulent structures can be seen from the instantaneous temperature contours, where the higher temperature shear layer can be seen to grow immediately from the nozzle lip.

Time averaged axial velocity profiles are compared with the UTRC experiment in Fig. 7 and 8. The time averaged LES flow predictions improve with successive grid refinement. The coarse grid over-predicts large scale mixing and the jet decays too quickly. The finest grid captures the over-all growth rate of the shear layer and also the appropriate centerline decay rate and plume length. At $15D_J$ downstream, the radial profile of the plume agrees with the experimental measurements.

Near-field sound was recorded in the UTRC experiment on a rotating microphone array ranging from x=1 to $13D_J$. The first microphone is located at 0.97 D_J from the centerline and the last is located at 2.5 D_J, with a spread angle of approximately 7°, and each microphone is separated axially by 1.2 D_J. The FW-H surfaces were used to extract the near-field microphone spectra from the LES calculations. These FW-H surfaces are slightly closer to the shear layer than the microphones in the UTRC experiment. Figure 9 compares the $x = 1.1267D_J$ microphone with

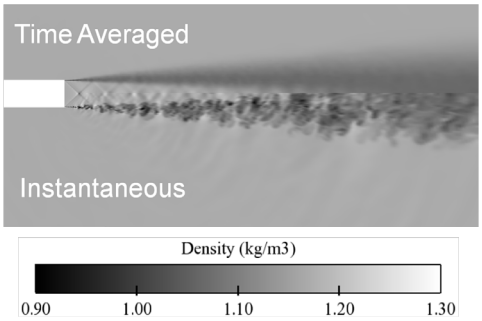

FIGURE 5. LES DENSITY CONTOURS, TIME AVERAGED (TOP), INSTANTANEOUS (BOTTOM)

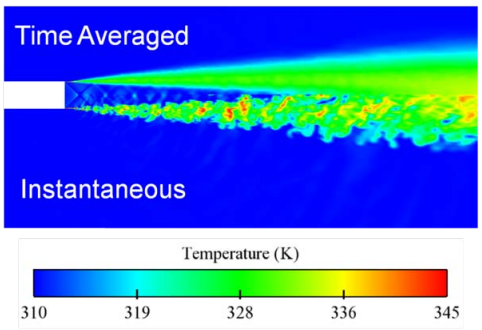

FIGURE 6. LES TEMPERATURE CONTOURS, TIME AVERAGED (TOP), INSTANTANEOUS (BOTTOM)

the LES calculations and Fig. 10 compares the microphone located at $x = 6.1267D_J$. The spectral levels are unpublished in the literature for the current case [24], therefore the figures are the CRAFT Tech levels uniformly scaled to fit the published spectral shape, and the experimental spectra should be considered qualitative reference only. In general, the near-field spectral shapes agree well at both compared locations. The medium LES calculation over-predicts the higher frequencies close to the nozzle lip, possibly due to the location of the FW-H surface. However, similar tones and broadband spectral shape is captured by the LES at all grid densities. As mentioned previously, the coarse grid greatly over-predicts large scale mixing and this is reflected by the over-prediction of low frequency noise in the downstream microphone.

Far-field Noise Calculations

Far-field noise calculations were performed for all three grid densities and compared with the measurements at UTRC. Nine microphones measure the far-field noise at unequal radial distances from the jet exit. The lowest elevations are at the downstream end of the jet, and the higher angles are upstream, where 90° is the transverse direction. A limitation to the current method is the inability to model the secondary shear layer created by the open jet exhausting into still air. The far-field microphones in the UTRC experiment were located outside of this secondary shear layer in still air, so the corresponding FW-H calculation

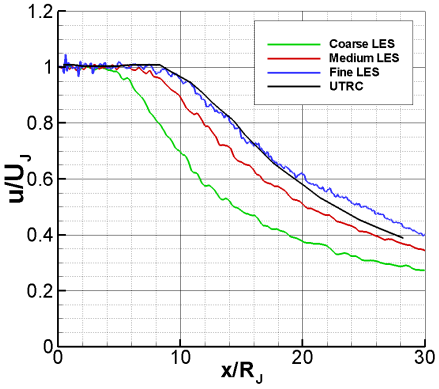

FIGURE 7. CENTERLINE VELOCITY PROFILES FOR MACH 1.5 JET

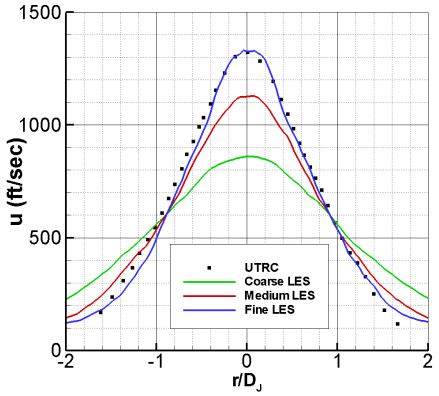

FIGURE 8. RADIALLY VARYING MEAN AXIAL VELOCITY AT x=15D_J

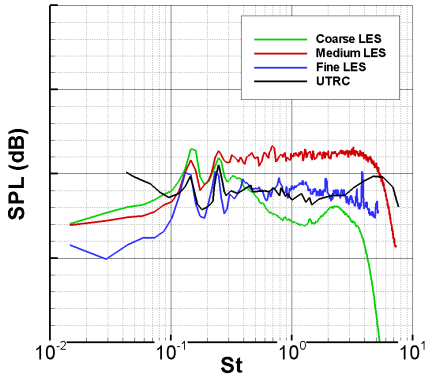

FIGURE 9. NEARFIELD SPL FOR UTRC TEST CASE B118 ($x/D_J = 1.1267$)

consisted of a stationary FW-H surface and stationary far-field microphones. However, the affects of the secondary shear layer on the primary jet noise radiation are unknown. Figure 11 is a comparison of the far-field OASPL directivity with the experiment [25] for all three grid densities. Although the directivity

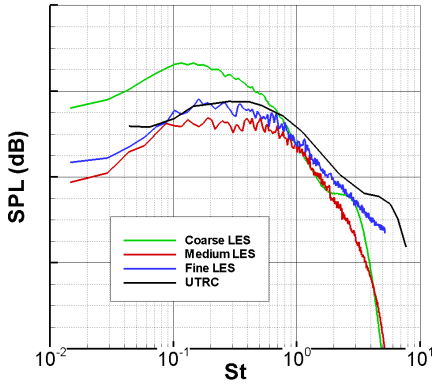

FIGURE 10. NEARFIELD SPL FOR UTRC TEST CASE B118 (x/D_J = 6.1267)

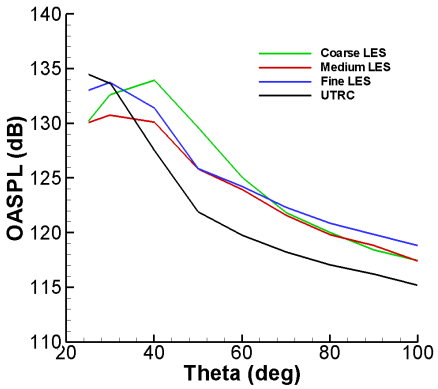

FIGURE 11. FAR-FIELD OASPL DIRECTIVITY COMPARISON

pattern agrees between the LES and experiment, there is a 3-5 dB disagreement between all three grid densities and the experiment at upstream angles. The fine LES calculation predicts the greatest noise at downstream angles around 25°, possibly due to the increased resolution of turbulent structures downstream. Far-field spectra are compared in Fig. 12 and 13 for the 25° and 60° microphones, respectively. Similar to the near-field spectra, the UTRC levels were not published so the results shown are scaled to match the spectral shape of the experiment. The experimental curves are for qualitative reference only. As expected, the finer grids increase the SPL prediction in the higher frequencies. The spectral shape in the 25° direction agrees well with the experiment including the peak frequency and the approximate spectral decay. Moving upstream at 60°, the coarse grid greatly over-predicts the lower frequency spectrum relative to the medium and fine grids. Also, the medium and fine grid spectra peak at a higher frequency than the experimental measurements. These findings are very similar to the far-field predictions found in the literature [24] using a similar LES/FW-H method.

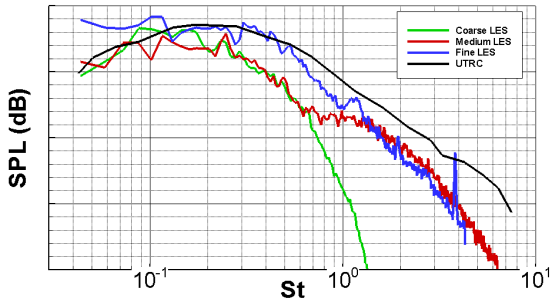

FIGURE 12. FAR-FIELD SPECTRUM COMPARISON AT 25° FOR MACH 1.5 JET

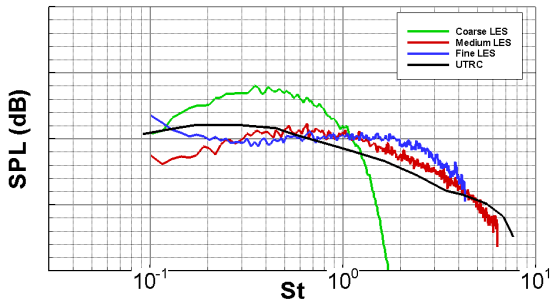

FIGURE 13. FAR-FIELD SPECTRUM COMPARISON AT 60° FOR MACH 1.5 JET

TWIN LABORATORY JET

Real world military gas turbine engines are often installed in twin jet configurations. CRAFT CFD® is a multi-block code that allows for the use of structured grids with the detailed topology required when simulating two independent jet plumes. A full three-dimensional twin jet plume was simulated with LES and compared with an experiment performed at University of Mississippi's National Center for Physical Acoustics (NCPA) jet noise facility. The twin jets are heated and over-expanded with a jet exit centerline Mach number of approximately 1.58. The non-uniform nozzle exit profile was calculated previously with a RANS analysis of the laboratory nozzles, including a realistically shaped center body and cooling layers. The nozzle lips consist of twelve flat facets and the jet axes are canted inward at a total angle of four degrees. The faceted nozzle twin O-H topology is shown in Fig. 14. The twin jet grid extended $30D_J$ downstream before the application of a buffer zone, and consisted of around nine million grid cells. The near-field statistics are examined from the LES as well as the associated far-field noise predictions with the FW-H method. Differences in both the time-averaged flowfield and the far-field noise are examined in the transverse and sideline direction, where the directional terminology is illustrated in Fig. 15.

Twin Laboratory Jet LES

The twin jet configuration was simulated until statistical convergence at various locations in the jet plume before sampling

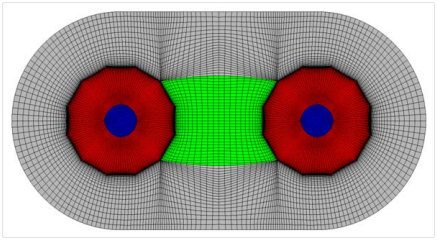

FIGURE 14. TWIN O-H GRID TOPOLOGY: H-GRIDS (BLUE, GREEN, GREY) AND O-GRIDS (RED)

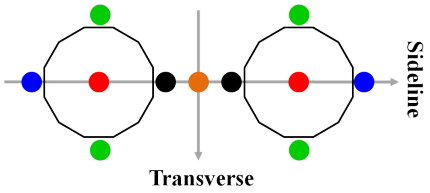

FIGURE 15. LOCATION OF LINE SEGMENTS IN TWIN JET PLUME: JET AXIS (RED), UPPER/LOWER LIPLINE (GREEN), OUTER LIPLINE (BLUE), INNER LIPLINE (BLACK), CENTERLINE (ORANGE)

for mean flow features and far-field noise. After convergence, the jet was simulated for 0.04 seconds which corresponds to about ten domain flow-thru times, assuming a convection velocity of half the jet exit velocity. Figure 16 is a top view of time averaged and instantaneous Mach number contours. Multiple jet plume shock cells are resolved by the LES and the two plumes start interacting as soon as $2D_J$ downstream. Temperature contours are shown in Fig. 17, where the unsteady shear layers generate large scale structures that mix rapidly downstream. Self similarity of the combined jet plumes occurs after $30R_J$ downstream. Figure 18 and 19 are plots of normalized axial velocity versus radial distance (transverse and sideline directions) for varying downstream locations. The axial velocity (u) is normalized by the centerline axial velocity (u_c), and the radial location is normalized by the radial location where $u = 0.5u_c$. The profiles are very similar in both the transverse and sideline direction.

Time-averaging of the unsteady simulation was calculated from 200 instantaneous solutions. Axial velocity and turbulent kinetic energy (TKE) levels were calculated on line segments starting at the nozzle exit plane (starting locations of the line segments are shown in Fig. 15) and extending downstream to $30D_J$. The lipline segments originate at $r = 1.1R_J$. Averaging was performed for symmetric line segments (identical colors) to smooth the plots. All of the line segments originate at the jet exit plane and are canted inward at an angle of 2°, except for the centerline segment which is directed straight downstream. These colors are coordinated with the axial velocity plots in Fig. 20 and the TKE plots in Fig. 21.

A few key points can be made from the time averaged axial velocity plots. First, many strong shock cells are captured by the LES along the jet axis. The over-expanded operating con-

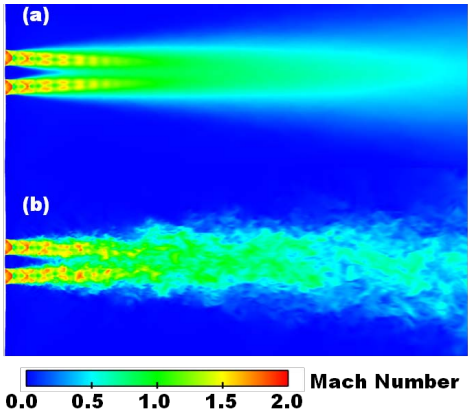

FIGURE 16. MACH NUMBER CONTOURS FOR HEATED TWIN JET (A)INSTATNANEOUS (B)TIME AVERAGED

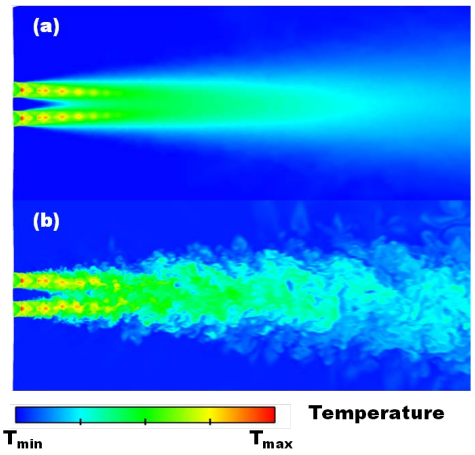

FIGURE 17. TEMPERATURE CONTOURS FOR HEATED TWIN JET (A)INSTATNANEOUS (B)TIME AVERAGED

dition of the nozzles generate strong shocks that are expected to interact with the shear layer and create substantial upstream directed shock noise. The centerline plot indicates plume interaction around $2D_J$, and the maximum convective velocity along the jet centerline is $0.5U_J$ at $9D_J$ downstream. There is little difference in axial velocity profiles along the upper/lower and outer liplines, suggesting that the growth and decay rate in the sideline and transverse directions is similar, consistent with the self-similar profiles of Figures 18 and 19.

Turbulent kinetic energy levels are shown in Fig. 21. The highest TKE levels occur along the inner lipline at $2D_J$ downstream, indicating that the jets are interacting very strongly with one another, compared with the lower TKE levels along the outer and upper/lower liplines where little interaction is expected. The peak mixing along the centerline of the two nozzles occurs around $12R_J$ downstream, but the individual plumes reach their peak levels afterwards around $15R_J$.

Near-field sound pressure levels were calculated at locations just outside of the twin jet shear layer in the transverse and side-

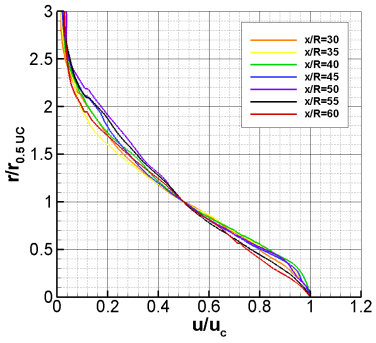

FIGURE 18. SELF-SIMILAR PROFILES OF JET PLUME IN TRANSVERSE DIRECTION

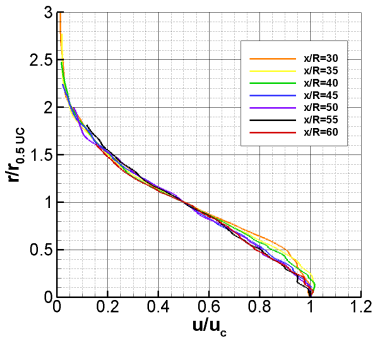

FIGURE 19. SELF-SIMILAR PROFILES OF JET PLUME IN SIDELINE DIRECTION

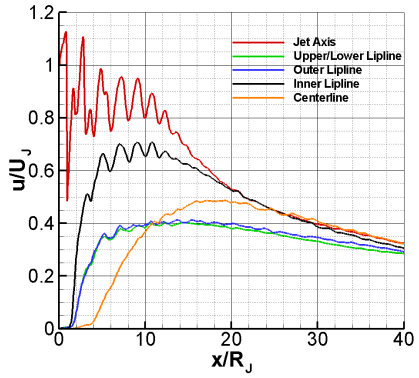

FIGURE 20. TIME AVERAGED AXIAL VELOCITY VERSUS DOWNSTREAM DISTANCE ALONG VARIOUS LINE SEGMENTS

line directions. Figure 22 shows the narrowband SPL spectra in the transverse and sideline directions at 4 and 8 D_J. A jet screech tone is well-resolved around 3.4 kHz at all microphone locations, and is stronger in the transverse direction than the sideline direction. In addition, a broadband shock-associated noise (BBSAN) component is strongest in the transverse direction at $4D_J$.

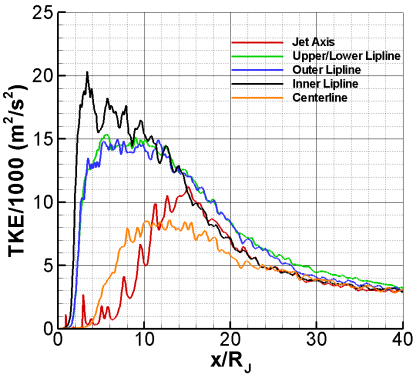

FIGURE 21. TKE VERSUS DOWNSTREAM DISTANCE ALONG VARIOUS LINE SEGMENTS

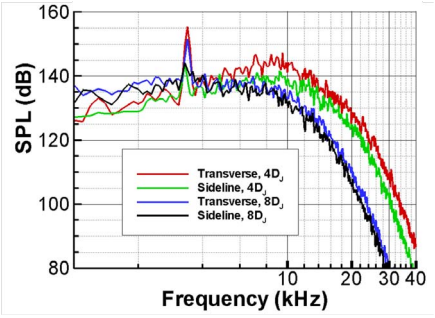

FIGURE 22. NEAR-FIELD SPL SPECTRA FOR TWIN JET

Far-Field Noise Calculations

The far-field noise of the twin jet configuration was calculated with the LES/FW-H method. The FW-H surface is wider in the sideline direction than the transverse direction to fit the oblong shape of the twin jet plume. Figure 23 and 24 show contours of dilatation and vorticity magnitude on planes perpendicular to the transverse and sideline directions, respectively. There are unique interference patterns in the two directions associated with the location and angle of the twin plumes. Differences in the far-field noise directivity and spectra are expected between the transverse and sideline directions.

The far-field OASPL directivity and SPL spectra are shown in Figures 25 through 28. Figure 25 is the plot of OASPL at a circular arc of radius $57.6D_J$ from the nozzle exit in the transverse and sideline directions, compared with the UTRC experiment. The peak level of approximately 140dB at an angle of 55° is captured excellently. The level falls off at the appropriate rate, and shock noise is captured at upstream angles greater than around 90°. The OASPL slope at 90° levels out and is identical to the trend found in the experimental data due to the upstream propagating shock waves. The under-prediction of SPL at the lower elevation angles which could be due to poor grid resolution at this location on the FW-H surface. Figures 26 and 27 are narrowband spectra for the jet in the shock noise direction. The CRAFT Tech calculation resolves the jet screech tone at approximately 3.2 kHz. Also, the BBSAN follows the trend in the experimental

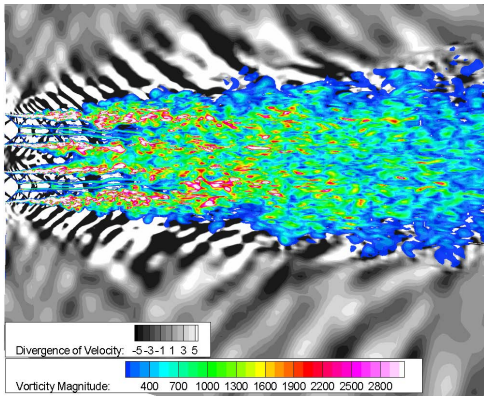

FIGURE 23. TOP VIEW OF DILATATION FIELD FOR TWIN JET

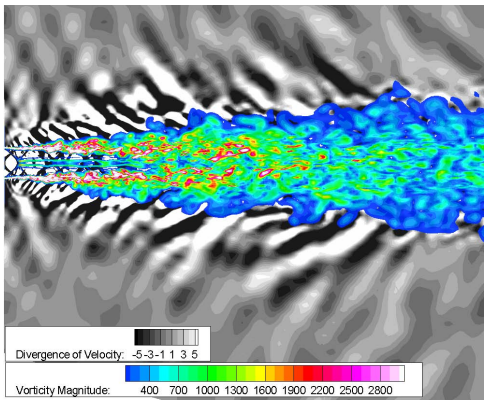

FIGURE 24. SIDE VIEW OF DILATATION FIELD FOR TWIN JET

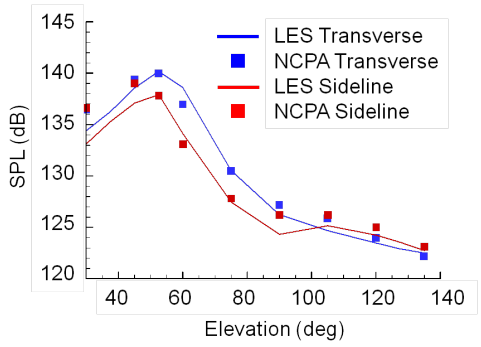

FIGURE 25. TWIN JET OASPL DIRECTIVITY

measurements. Figure 28 is the narrowband spectrum for an observer located in the downstream (Mach wave) direction. There is little spectral difference in the Mach wave direction between the sideline and transverse directions, so the spectra at this elevation are shown azimuthally averaged and the peak SPL and spectral shape agrees with the experiment. Higher frequencies are over-predicted in both the upstream and downstream angles, consistent with the Mach 1.5 jet noise. The sources of this over-prediction are a topic of continuing research.

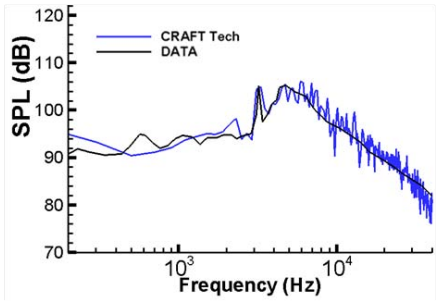

FIGURE 26. UPSTREAM TWIN JET SPECTRUM (SIDELINE)

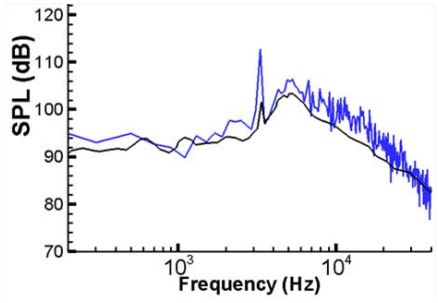

FIGURE 27. UPSTREAM TWIN JET SPECTRUM (TRANSVERSE)

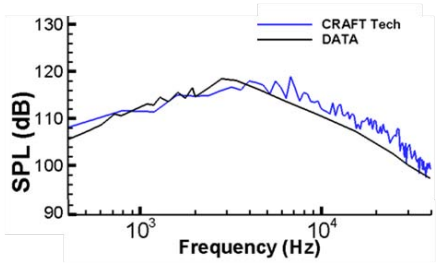

FIGURE 28. TWIN JET SPECTRUM IN MACH WAVE DIRECTION

CONCLUSIONS AND FUTURE RESEARCH

This paper presented a method to predict far-field noise emitted by supersonic jet exhausts. High fidelity LES using CRAFT CFD® was coupled with a far-field acoustic solver via the FW-H equation. The LES has been examined in the near-field of a pressure-balanced, isothermal, Mach 1.5 jet, followed by comparisons of far-field noise with experimental measurements at UTRC. The CRAFT Tech near and far-field noise predictions agree fairly well with experimental measurements, but the over-prediction of upstream noise is a topic for further research. Certain features of the TKE profiles predicted by the LES, especially close to the nozzle lip, are suspected in the over-prediction of high frequency far-field noise. The heated twin jet LES was simulated with a twin O-H grid topology. The far-field noise predictions agree well with experimental measurements at NCPA. In addition to far-field noise, near-field statistics and mean flow

were shown and give insight to the twin jet flowfield.

Careful near-field analysis should be performed before looking at far-field noise with the FW-H method. In the current work, near-field flow features were identified that directly affect the far-field noise. When available, mean flow and near-field microphone measurements from experiments compliment far-field noise measurements, and are useful when validating the LES/FW-H predictions. Relating the near-field features of supersonic jet plumes to their far-field acoustic signatures is necessary when designing noise reduction concepts of interest to the United States Navy.

ACKNOWLEDGMENT

This work was supported by a NAVAIR Propulsion & Power STTR award.

REFERENCES

[1] Naval Research Advisory Committee, 2009. Report on jet engine noise reduction, April.

[2] Bridges, J., Wernet, M., and Brown, C., 2003. Control of jet noise through mixing enhancement. Tech. Rep. TM 2003 212335, NASA.

[3] Krothapalli, A., Venkatakrishnan, L., Lourenco, L., Greska, B., and Elavarasan, R., 2003. "Turbulence and noise suppression of a high-speed jet by water injection". *Journal of Fluid Mechanics,* ***491***, pp. 131–159.

[4] Kumar, R., Lazic, S., and Alvi, F., 2009. "Control of High-Temperature Supersonic Impinging Jets Using Microjets". *AIAA Journal,* ***47***(12), pp. 2800–2811.

[5] Samimy, M., Kim, J.-H., Kastner, J., Adamovich, I., and Utkin, Y., 2007. "Active control of high-speed and high-reynolds-number jets using plasma actuators". *Journal of Fluid Mechanics,* ***578***, pp. 305–330.

[6] Lyrintzis, A., 2003. "Integral Acoustics Methods: From the (CFD) Near- Field to the (Acoustic) Far-field". *International Journal of Aeroacoustics,* ***2***(2), p. 95.

[7] Uzun, A., Lyrintzis, A., and Blaisdell, G., 2005. "Coupling of integral acoustics methods with LES for jet noise prediction". *International Journal of Aeroacoustics,* ***3***(4), pp. 297–346.

[8] Bodony, D., and Lele, S., 2006. "Review of the current status of jet noise predictions using Large-Eddy Simulation". 44th AIAA Aerospace Sciences Meeting and Exhibit, AIAA-2006-0468.

[9] Sinha, N., Erwin, J., Kannepalli, C., and Arunajatesan, S., 2010. "LES predictions of noise emissions from a low-bypass ratio military gas turbine engine". ASME Turbo Expo 2010, ASME Paper GT2010-22191.

[10] Sinha, N., Kenzakowski, D., Ungewitter, R., Dash, S., and Seiner, J., 2008. "Computational and Experimental Investigations of Jet Noise Reduction Concepts for Low Bypass Ratio Military Gas Turbine Engines". ASME Turbo Expo 2008, ASME Paper GT2008-50091.

[11] Arunajatesan, S., and Sinha, N., 2003. "Hybrid RANS/LES Modeling for Cavity Aeroacoustics Predictions". *Journal of Aeroacoustics,* ***2***(1), pp. 65–93.

[12] Kannepalli, C., Arunajatesan, S., and Dash, S., 2002. "RANS/LES Methodology for Supersonic Transverse Jet Interactions with Approach Flow". AIAA-2002-1139.

[13] Calhoon, W. J., Kannepalli, C., Arunajatesan, S., and Dash, S., 2002. "Analysis of Scalar Fluctuations at High Convective Mach Numbers". AIAA-2002-1087.

[14] Kim, W., and Menon, S., 1995. "A New Dynamic One-Equation Subgrid Scale Model for Large Eddy Simulation". AIAA-1995-0356.

[15] Sinha, N., Arunajatesan, S., Kannepalli, C., Erwin, J., and Dash, S., 2009. "Unified RANS/LES Engineering Framework for Predicting Jet Structure and Noise for Realistic Aircraft Exhausts". ONR Advanced Propulsion Conference.

[16] Farassat, F., 2007. Derivation of Formulations 1 and 1A of Farassat. Tech. Rep. NASA/TM-2007-214853, Langley Research Center, Hampton, VA.

[17] Ffowcs Williams, J., and Hawkings, D., 1969. "Sound Generated by Turbulence and Surfaces in Arbitrary Motion". *Philosophical Transactions of the Royal Society,* ***A24***, pp. 321–342.

[18] Brentner, K., and Farassat, F., 1998. "An Analytical Comparison of the Acoustic Analogy and Kirchhoff Formulation for Moving Surfaces". *AIAA Journal,* ***36***(8), pp. 1379–1386.

[19] di Francescantonio, P., 1997. "A new boundary integral formulation for the prediction of sound radiation". *Journal of Sound and Vibration,* ***202***(4), pp. 491–509.

[20] Spalart, P. R., and Shur, M. L., 2009. "Variants of the ffowcs williams-hawkings equation and their coupling with simulations of hot jets". *International Journal of Aeroacoustics,* ***8***(5), pp. 477–492.

[21] Mendez, S., Shoeybi, M., Sharma, A., Lele, S. K., and Moin, P., 2009. "Post-processing of Large-Eddy Simulations for jet noise predictions". Center for Turbulence Research Annual Research Briefs.

[22] Shur, M., Spalart, P., and Strelets, M., 2009. "Noise prediction for increasingly complex jets. part i: Methods and tests". *International Journal of Aeroacoustics,* ***8***(5), pp. 477–492.

[23] Uzun, A., 2003. "3D Large Eddy Simulation for Jet Aeroacoustics". PhD Thesis, Purdue University.

[24] Khalighi, Y., Ham, F., Moin, P., Lele, S., Colonius, T., Schlinker, R., Reba, R., and Simonich, J., 2010. "Unstructured Large Eddy Simulation Technology for Prediction and Control of Jet Noise". Proceedings of ASME Turbo Expo 2010: Power for Land, Sea and Air, GT2010-22306.

[25] Schlinker, R., Simonich, J., Shannon, D., Reba, R., Colonius, T., Gudmundsson, K., and Ladeinde, F., 2009. "Supersonic jet noise from round and chevron nozzles: Experimental studies". AIAA-2009-3257.